Impact of Solvent Vapor Annealing on the Morphology and Photophysics of Molecular Semiconductor Thin Films

John C. Conboy,[†] Eric J. C. Olson,[†] David M. Adams,[†] Josef Kerimo,[†] Arie Zaban,[‡] Brian A. Gregg,[‡] and Paul F. Barbara*,[†]

Department of Chemistry, University of Minnesota, 207 Pleasant Street SE, Minneapolis, Minnesota 55455, and The National Renewable Energy Lab, 1617 Cole Boulevard, Golden, Colorado 80401

Received: February 3, 1998; In Final Form: April 6, 1998

The effect of solvent vapor annealing on the fluorescence properties and morphology of titanyl phthalocyanine/perylene phenethylimide thin-film molecular semiconductor bilayers (TiOPc/PPEI) is investigated. A combination of atomic force microscopy (AFM) and near-field scanning optical microscopy (NSOM) is used in conjunction with bulk absorption and fluorescence measurements to correlate the morphological and photophysical properties of these bilayer systems. AFM data show that treatment of the vacuum-deposited amorphous PPEI and TiOPc/PPEI films results in the crystalline transformation of these materials and severely alters the contact between the TiOPc and PPEI layers. AFM data show extended solvent vapor annealing produces void spaces in the TiOPc coverage on the order of several hundred nanometers. Steady-state fluorescence intensity and fluorescence lifetime measurements are used as a measure of charge-transfer quenching efficiencies. Very efficient charge-transfer quenching is observed when amorphous layers of TiOPc are deposited onto PPEI resulting from uniform contact between the layers. Extended annealing results in decreased charge-transfer quenching efficiencies as a result of widely dispersed, localized interfacial contact points.

Introduction

Molecular-based semiconductor materials have unique electronic and optical properties and offer tremendous flexibility and tunability in processing. They are currently being utilized in a wide range of devices including photovoltaic solar cells, light-emitting diodes, and chemical sensors.[1−9] While these devices have not yet been commercialized, molecular-based semiconductors have been extensively applied in commercial electrophotography (photocopying) for several decades.[6] At the heart of many of these devices is a heterojunction between n-like and p-like molecular semiconductor layers (n-MSL and p-MSL). As with classical inorganic semiconductor devices, this n−p junction is the basis for the devices' properties (be it light emission from an applied potential or the production of an electrical potential via light absorption). A typical molecular-based solar cell is shown in Figure 1. Absorption of light by the n-MSL results in the production of mobile singlet excitons which may diffuse to the n−p interface and undergo electron transfer across the interface, i.e., charge-carrier generation. The energy difference between the molecules at the interface is the driving force for the charge-carrier generation process. The rates and efficiencies of many "primary processes" such as exciton diffusion/migration to the interface, the kinetics of electron transfer across the interface, the dissociation of the charge-transfer state into free carriers, and the "energy-wasting" radiative and nonradiative decay of excitons en route to the interface effect the charge-carrier generation process.[10−18] It is believed that these primary processes are strongly influenced
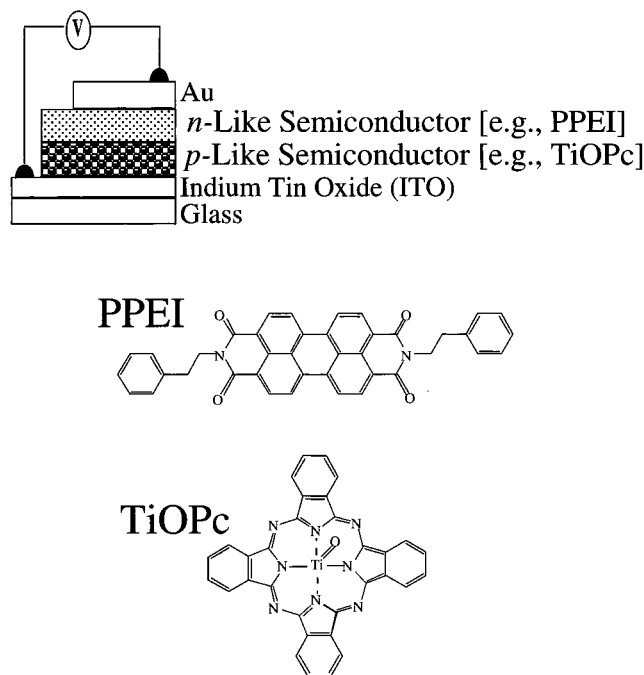

Figure 1. Schematic of a typical molecular semiconductor-based photovoltaic device. Also shown are the chemical structures of perylene phenethylimide (PPEI) and titanyl phthalocyanine (TiOPc).

by the complex nanoscale and mesoscale morphologies of the n-MSL, p-MSL, and the interfacial region.

Thin-film morphologies are highly dependent on the methods and conditions of film preparation.[9,19] Vacuum deposition, spin-casting, and solution-phase self-assembly techniques are used to produce molecular semiconductor thin-film assemblies for

* To whom correspondence should be addressed.
† University of Minnesota.
‡ NREL.

Molecular Semiconductor Films

J. Phys. Chem. B, Vol. 102, No. 23, 1998 **4517**

device applications. In particular, vacuum deposition is commonly used to prepare layered assemblies of molecular materials with extremely uniform thickness and efficient contact between layers. Deposition parameters such as substrate temperature and evaporation rates can greatly effect the film morphology.[9] Moreover, postdeposition processing techniques including solvent annealing, solvent vapor annealing, and thermal annealing can often be used to restructure thin-film morphologies by inducing crystallization.[6,19−21] In some cases, various postdeposition processing techniques have been observed to produce different crystalline transformations.[22] Indeed, postdeposition processing has been shown to improve the electrophotographic,[6,20] photovoltaic,[23−26] photoconductive,[20,27] and photoelectrochemical[19,21,28] properties of thin-film devices. The improved photophysical and electronic properties of these materials have been attributed to increased exciton migration lengths and charge carrier mobilities, alterations of the optical and/or electronic band structures, and other factors. In a recent study, increased exciton migration lengths in solvent vapor-annealed perylene phenethylimide/titanyl phthalocyanine bilayer (PPEI/TiOPc) assemblies were attributed to the crystallinity of the PPEI layer.[26] It is important to point out that in certain cases postdeposition annealing over extended periods has been reported to degrade device performance, especially for thin bilayers.[7] In a recent study, we used the high topographical and optical/spectroscopic resolution of near-field scanning optical microscopy (NSOM) to spatially resolve the complex morphologies, spectroscopy, and charge-transfer-induced fluorescence quenching efficiencies of PPEI/TiOPc assemblies.[14] Extended solvent vapor annealing of the assemblies was responsible for (i) the formation of pinholes, (ii) reduced effective interfacial contact area, and (iii) attenuated charge-transfer fluorescence quenching efficiency between the n-MSL and p-MSL in PPEI/TiOPc assemblies.[14] Such transformations of molecular semiconductor layers and the interfacial region are expected to have an impact on device performance.

This paper extends our previous study[14] of molecular-based semiconductor materials. These studies were undertaken to obtain a higher spatial resolution topographic picture of the interface between vacuum-deposited and solvent vapor-annealed thin films and to obtain quantitative information on the extent of interfacial contact, nanocrystalline size distributions, and fluorescence properties. High-resolution atomic force microscopy (AFM) is used in conjunction with NSOM and conventional fluorescence and absorption spectroscopy to determine the effect of solvent vapor annealing on nanoscopic structure and charge separation efficiency of bilayer films of TiOPc and PPEI. In the previous studies, thin-film bilayer assemblies were formed by depositing PPEI on top of TiOPc films (denoted PPEI/TiOPc). This study investigates these films as well as films prepared in the reverse order where TiOPc is deposited on top of PPEI (TiOPc/PPEI). AFM, NSOM, optical absorption, and fluorescence measurements are used to probe the change in electronic properties of the materials at various stages of solvent vapor-induced restructuring. Fluorescence lifetimes and quantum yields are measured in the presence and absence of the TiOPc quencher. Fluorescence measurements provide an indirect measure of charge separation efficiency since the primary exciton quenching mechanism is due to charge transfer at the PPEI−TiOPc interface.[10−13] The examination of PPEI/TiOPc and TiOPc/PPEI bilayers and PPEI single layers has led to a nanoscopic picture of how vacuum deposition and subsequent solvent vapor annealing controls the local structure and subsequent optical/electronic properties of these films.

Experimental Section

Materials. Perylene phenethylimide, PPEI (structure shown in Figure 1), was synthesized and purified as reported previously.[26] Titanyl phthalocyanine, TiOPc (structure shown in Figure 1), was purchased from H.W. Sands Corp. Glass microscope coverslip substrates were dehydrated prior to use by baking at 150 °C for at least 1 h. The slides were then transferred directly to the evaporation chamber. PPEI and TiOPc were separately evaporated in a vacuum at ∼10^{-7} Torr onto substrates at room temperature by a method previously described.[26] Films of a single layer of PPEI were prepared as well as TiOPc/PPEI and PPEI/TiOPc bilayers. PPEI-only layers and TiOPc/PPEI bilayers were prepared on the same substrate in order to make comparisons between the single and bilayer films. Films were solvent vapor annealed by placing a small open container of methylene chloride beneath the film coated substrates in an airtight container.

TiOPc/PPEI Bilayers. The PPEI film (14 nm) was vacuum deposited first and then annealed in methylene chloride vapor for 3 days. A portion of the coverslip (substrate) was masked prior to the subsequent deposition of a TiOPc (7 nm) overlayer, allowing for both a single layer of PPEI and bilayer of TiOPc/PPEI to be present on the same sample. The films were then solvent vapor annealed in a methylene chloride/air environment at room temperature for the various times described below.

PPEI/TiOPc Bilayer. This film was prepared in an analogous manner to the previous. TiOPc (10 nm) was first vacuum deposited onto a masked glass substrate and annealed for 24 h. PPEI (30 nm) was then vacuum deposited, and the entire bilayer was annealed for 48 h.

AFM and NSOM Measurements. AFM measurements were performed with a Topometrix Explorer AFM. The AFM was operated in contact mode. The samples were not altered by this measurement, as noted by the invariance of successive AFM scans. NSOM measurements were performed on a modified Topometrix Aurora I. The apparatus and analogous experimental methods have been described in detail elsewhere.[14,29−34] NSOM probes were produced in house. A 630 nm single-mode optical fiber (3M) was pulled using a Sutter P-2000 pipet puller. Aluminum was vapor deposited onto the probes under vacuum at a pressure of 5×10^{-6} Torr. NSOM measurements performed on numerous occasions, with different NSOM tips, in different regions of the sample, or with different samples, were observed to be highly reproducible and not subject to artifacts due to sample heating by the NSOM probe or photolysis of the samples by the near-field excitation. Bulk fluorescence measurements were performed on a SPEX fluorimeter. UV−visible absorption experiments were performed on a Shimadzu UV160U spectrophotometer.

Lifetime Measurements. Emission decays were obtained by time-correlated single-photon counting techniques. Excitation pulses centered near 420 nm were produced by a cavity-dumped Ti:sapphire laser frequency-doubled with a β-BBO crystal. Aluminum-coated (NSOM probes) and uncoated tapered optical fibers were employed to deliver the excitation to localized regions of the sample. Detecting the total PPEI emission band with our multichannel plate photomultiplier tube (Hamamatsu, RU3809U-01) produced a slight spectral bias, with maximum detector sensitivity on the blue edge of the PPEI emission spectrum. Emission decays were accumulated in a multichannel analyzer (TRACOR Northern, 7200), transferred to a PC, and fit utilizing a weighted-residuals nonlinear least-squares fitting routine. Under our experimental NSOM conditions, the far-field and near-field lifetime measurements are

identical within experimental error, indicating very little if any tip quenching. Lifetime measurements were reproduced with different tips, in different regions of the sample, and showed typical χ^2 values of 1.2−1.0. For comparison, emission decays are represented by $\tau_{avg} = \sum A_1\tau_1 + A_2\tau_2 + A_3\tau_3$, divided by the total amplitude of the three-exponential fit.

Results and Discussion

This paper is a complement to our previously reported NSOM investigation of PPEI/TiOPc bilayer assemblies.[14] AFM is used in this study to elucidate a higher spatial resolution topographical picture of the effect of solvent vapor annealing on the thin-film morphologies of PPEI/TiOPc and TiOPc/PPEI bilayer assemblies. Furthermore, a quantitative assessment of the impact of this modified morphology on the efficiency of charge-transfer quenching at the interface is obtained by combining AFM and NSOM with bulk absorption and fluorescence measurements (time-resolved and steady state). Quantitative information on the extent of interfacial contact, nanocrystalline size distributions, and fluorescence properties is presented. The complex morphologies of PPEI, PPEI/TiOPc, and TiOPc/PPEI thin films have been characterized at different levels of solvent vapor annealing. Very efficient charge-transfer quenching is observed when amorphous layers of TiOPc are deposited onto PPEI, which is the result of favorable energetics and high effective contact area. Charge-transfer quenching efficiency is severely degraded as these bilayer films are annealed, primarily resulting from the formation of well-dispersed, localized interfacial contact points. It is shown that in some cases solvent vapor annealing of bilayers with a TiOPc overlayer can lead to the formation of a different polymorph of PPEI. The use of high-resolution AFM and NSOM in conjunction with bulk spectroscopic techniques is shown to be a powerful method to study the effect of nanoscale morphology on the charge-transfer quenching efficiencies in molecular semiconductor heterojunctions.

The process of solvent vapor annealing is not well understood. Environmental factors in the annealing chamber, such as temperature gradients and levels of humidity, are difficult to control and can have a dramatic effect on the annealing process. As a result, the amount of annealing vs annealing time is not reproducible using our annealing procedure. Nevertheless, the general features of the film morphology and the spectroscopic characteristics of the TiOPc−PPEI bilayer systems are similar for different annealing runs.

Atomic Force Microscopy. The AFM data clearly show that solvent vapor annealing leads to the evolution of microcrystals from the initially amorphous vacuum-deposited films. AFM images of a PPEI film (14 nm, annealed in CH_2Cl_2 vapor for 3 days) and the same PPEI film with a 7 nm overlayer of unannealed TiOPc are shown in Figure 2, a and b, respectively. The topography after subsequent solvent vapor annealing with CH_2Cl_2 vapor for 30 min and 2 h are shown in Figure 2, c,d and e,f, respectively. Comparison of AFM images a and b reveals only subtle differences between the two films, suggesting that the unannealed TiOPc forms a completely amorphous film and adapts to the substrate contour, in this case the PPEI nanocrystals. The PPEI nanocrystals shown in Figure 2a have the following mean dimensions: length 500 ± 125 nm, width 70 ± 20 nm, and height 15 ± 4 nm. A number of pinholes are also apparent, most likely formed during initial solvent vapor annealing. The percentage of exposed substrate or pinholes for the PPEI film and for the TiOPc/PPEI bilayer are 15± 3% and 8 ± 2%, respectively. The lower percentage of void space in

the TiOPc/PPEI bilayer is most likely due to the additional thickness resulting from the TiOPc overlayer. Figure 2c,d displays the transformation seen upon solvent-vapor annealing of the film for 30 min. For PPEI alone, the nanocrystals are seen to increase slightly in size (e.g., compared to Figure 2a). In addition, there is a simultaneous increase in the exposed substrate area from 15% to 18% for the PPEI film. The transformation of the TiOPc/PPEI bilayer is even more striking. The initially amorphous TiOPc overlayer is restructured into nanocrystallites, ∼85 ± 32 nm in size, with a height of ∼25 ± 9 nm, which coat the PPEI surface and obscure the underlying PPEI crystals.

A dramatic transformation is observed upon further solvent vapor annealing and is illustrated in the AFM images of Figure 2e,f. The annealed PPEI and TiOPc/PPEI films display crystals of PPEI with fairly uniform size distributions. The single layer of PPEI (Figure 2e) is characterized by isolated long needlelike crystals of PPEI and numerous pinholes. The PPEI crystals have the following dimensions: 1500 ± 900 nm length, 190 ± 74 nm width, and 30 ± 16 nm height. Roughly 28% of the surface is exposed on this highly annealed "film". SEM micrographs of thermally annealed PPEI on SnO_2 have shown the same elongated crystallites (up to a few microns long) having their long axes in a direction roughly parallel to the substrate surface.[9] The AFM data for the TiOPc/PPEI bilayer (Figure 2f) show an almost continuous film of small TiOPc crystals (∼100 nm across and 30 nm high) and larger very disperse PPEI crystals. In addition, the geometric shape of the PPEI crystals is considerably different from those deposited on glass in the absence of TiOPc. These crystals appear more boxlike than the needlelike crystals found in the single layer of PPEI. The PPEI crystals formed with TiOPc present are not as long, with an average length of 900 ± 120 nm. The crystals are also more symmetric, having almost the same width (175 ± 85 nm) and height (125 ± 70 nm), compared to the PPEI crystals formed on glass. In addition, the coverage of PPEI crystals on the surface is significantly less for the TiOPc/PPEI bilayer where only 14% of the surface is covered compared with 72% for a PPEI-only film. It is likely that the large crystals of PPEI shown in Figure 2f are of a different polymorphic form than the ones formed on glass.

The needlelike crystals formed on glass can also be formed in the presence of TiOPc. Figure 3a,b shows the topography of a preannealed vapor-deposited PPEI film (48 nm, 3 days in CH_2Cl_2) with a 10 nm thick layer of TiOPc which has been subsequently annealed for 3 h. Isolated nanocrystals of TiOPc occur along the edges of the PPEI crystals or in the crevasses between crystals. During the annealing process the TiOPc migrates away from the upper surface of PPEI and preferentially forms crystals at the step edges of the crystalline PPEI. These results dramatically show that extended solvent vapor annealing in these bilayer assemblies greatly reduces interfacial contact between TiOPc and PPEI. In fact, interfacial contact appears to be limited to extremely small regions.

AFM was used to determine the morphology of the reverse bilayer PPEI/TiOPc films studied previously.[14] Figure 4a,b displays topographical images of a 10 nm preannealed vapor-deposited TiOPc film with a 30 nm thick PPEI layer deposited on top which has subsequently been annealed for 24 h in methylene chloride vapor. The initial annealing of the TiOPc for 24 h, prior to vacuum deposition of the PPEI and secondary annealing, serves to crystallize the TiOPc and help maintain its crystalline integrity throughout the PPEI crystallization process. The AFM topographical images show that more than 26% of
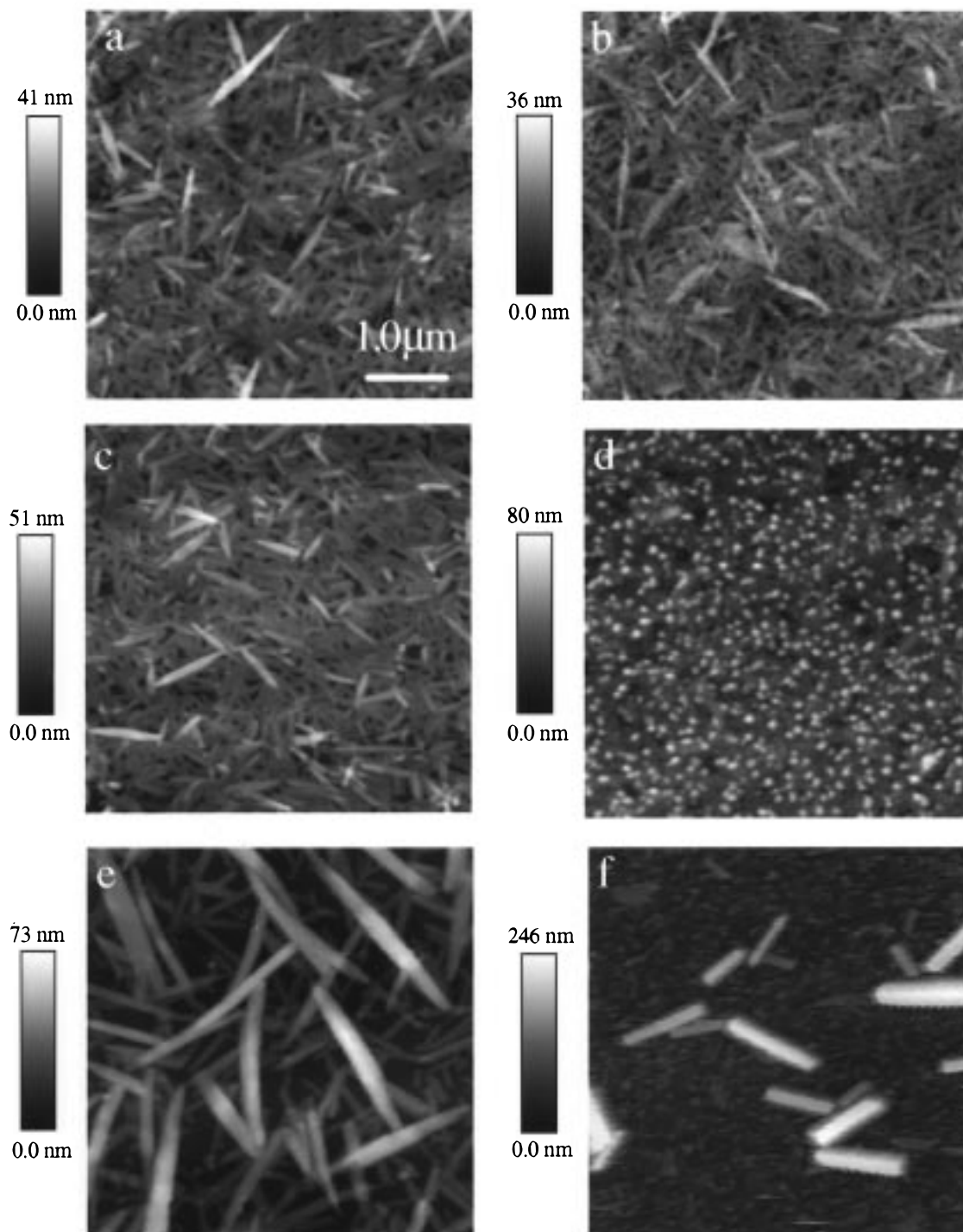
Figure 2. AFM topographical images of a 14 nm thick PPEI film, vapor annealed in methylene chloride for 3 days prior to vacuum deposition of a 7 nm thick TiOPc film. A mask was used during deposition of TiOPc to produce a region of the sample with no TiOPc. The AFM images follow the evolution of the films upon subsequent solvent vapor annealing. In the PPEI-only region of the sample, (a) initial sample, 0 min, (c) 30 min, and (e) 120 min. Corresponding images of the TiOPc/PPEI bilayer are shown in (b) 0 min, (d) 30 min, and (f) 120 min.

the film area is void of TiOPc and exists at the level of the substrate. These images also reveal well-defined TiOPc nano-crystals that have on average a typical in-plane cross section of 150−200 nm and an average height of 100 nm. The PPEI crystals display the same crystalline behavior observed in the PPEI-only films examined above. The PPEI crystals observed here have an average length of approximately 4.5 μm with heights ($\sim$225 nm) nearly half the size of their width ($\sim$400 nm). The interface between PPEI and TiOPc in these bilayers is limited to isolated contact points that are separated by hundreds of nanometers.

Solvent and thermal mediated processes have been used to induce amorphous/crystalline and crystalline/crystalline phase transitions and film transformations in a variety of materials. Certain phthalocyanine thin films have been shown to undergo an $\alpha-\beta$ phase transition when exposed to heat or organic solvents.[35,36] Sublimed films of magnesium phthalocyanine undergo a dimorphic phase change upon exposure to methylene chloride vapor.[23] Vacuum-deposited amorphous Ag films upon exposure to H_2O vapor form small crystalline domains.[37] In a thermal annealing process, the thermal energy added to the system is sufficient to overcome the surface free energy and
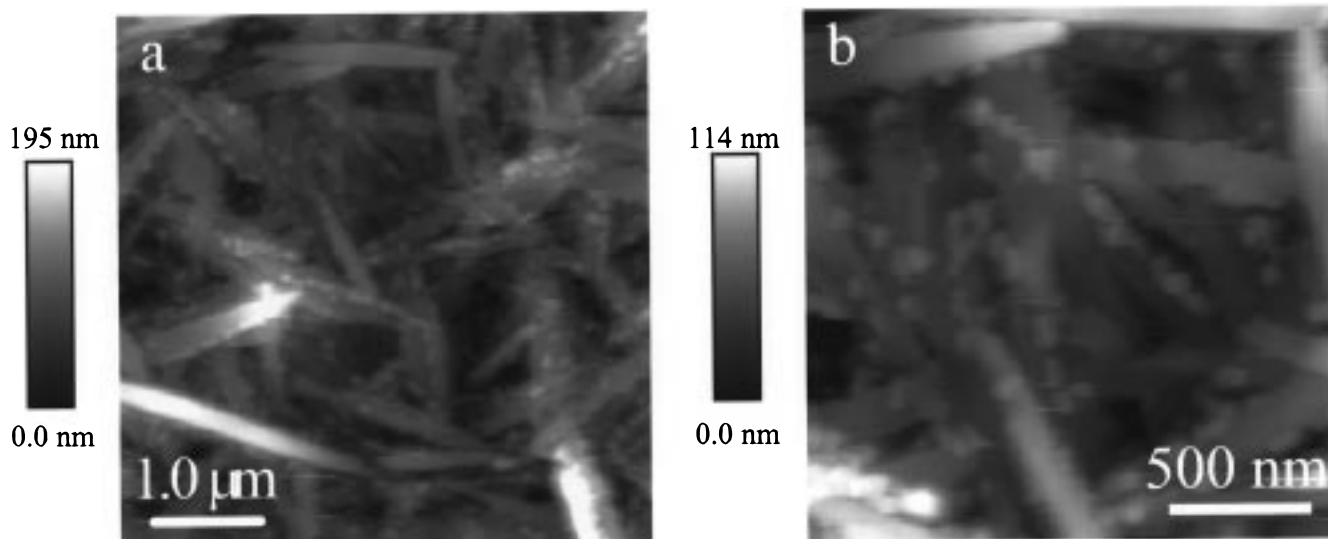
Figure 3. (a) AFM topographical image of a solvent vapor-annealed TiOPc/PPEI bilayer. The underlying ~40 nm thick PPEI layer was preannealed prior to deposition of 7 nm TiOPc. (b) A close-up of the same region showing the small TiOPc crystals between the larger PPEI crystals
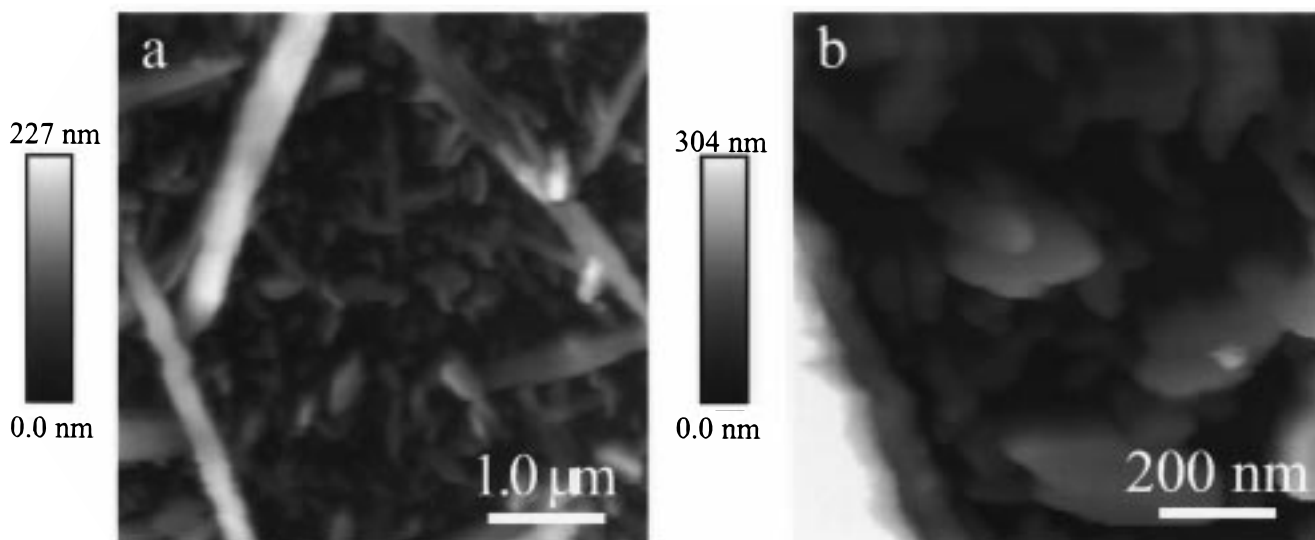

Figure 4. AFM topographic image of PPEI/TiOPc. The underlayer of TiOPc (10 nm) was preannealed and overcoated with 30 nm PPEI. The bilayer was then solvent vapor annealed for 3 days.

allow free movement of molecules on the surface or between crystals. In the case of solvent vapor annealing, the film is exposed to the vapor of a solvent in which the material has a very low to slight solubility. The effect of the solvent vapor is to reduce the effective surface free energy of the molecules and provide a convection medium for the transport of molecular species, similar to ripening of precipitates in solution.[38,39] Once a crystal nucleus has formed, the crystals grow until the entire amorphous layer has been transformed. At this point the crystals undergo ripening. According to the crystal ripening principles developed by Ostwald, the solubility of a crystal is dependent upon its size.[40] The smaller the crystal, the higher the solubility. This is a result of the change in the surface free energy for molecules on a small crystal versus those on a large crystal.[41,42] This process can account for the narrow size distribution of crystals observed in the AFM images of Figures 2−4. Crystals that have a particular "critical" size will have a solubility which is equal to that of the supersaturated vapor/solution above the surface. Crystals with a size smaller than the "critical" size will have a higher solubility and therefore a tendency to dissolve. Larger crystals will be the most insoluble and will have a tendency to grow. As Ostwald ripening continues, the size

distribution eventually becomes a stationary function that is independent of the original size distribution of the crystals.[38,39] It is this process which accounts for the uniform size distributions seen for both the TiOPc and PPEI crystals upon extended annealing.

Multiple polymorphs may exist for a single material. This is particularly true for perylenes for which many polymorphs are known.[6,22] It has previously been shown that the substrate and/or substrate condition plays an important role in the formation of a particular polymorph and/or distribution of crystals formed upon solvent vapor annealing.[9] In the bilayer films in the present study, the presence of TiOPc, the level of annealing of the starting layers, and the condition of the substrate have been shown to lead to the formation of distinct PPEI polymorphs. These factors likely influence the energetics and/or kinetics of Ostwald ripening, leading to the preferential development of one polymorphic form of PPEI over another. Interestingly, annealing with different solvents has a large effect on the annealing process. For example, acetone annealing has an effect similar to methylene chloride annealing but occurs more slowly. Annealing with methanol occurs even more slowly and has little effect on the degree of crystallization.
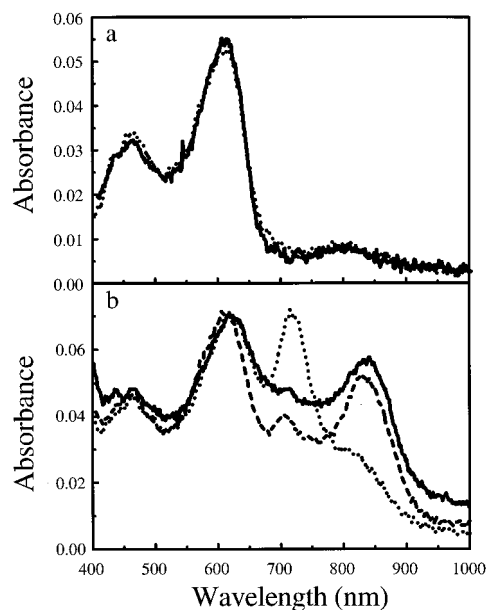
Molecular Semiconductor Films

J. Phys. Chem. B, Vol. 102, No. 23, 1998 **4521**

Figure 5. (a) Absorption spectrum of a vacuum-deposited PPEI film after annealing for 3 days (short dash) and after subsequent annealing for 120 min (solid line). (b) Absorption spectrum of a TiOPc/PPEI bilayer as a function of annealing time. Unannealed TiOPc film on a preannealed PPEI film (short dash) subsequently annealed 30 min (long dash) and then an additional 120 min (solid line).

Figure 6. PPEI absorption (short dash) and emission (solid line) spectra.

Absorption Spectra. The structural changes observed in Figure 2 are accompanied by discrete changes in the optical properties of both PPEI and TiOPc. Figure 5 shows the evolution of the absorption spectra of PPEI and TiOPc as a function of annealing time. Unannealed PPEI (not shown) displays broad absorption peeks at 460, 500, and 550 nm.[26] By analogy to 3,4,9,10-perylenetetracarboxylic dianhydride (PTC-DA), the succession of high-energy peaks from 500 nm on are attributed to the vibronic fine structure of the singlet S_1 manifold.[43] Specifically, the high-energy band in PTCDA has been assigned as a transition to a so-called S_1 Frenkel-like state (i.e., the excitation is confined to the monomer), while the low-energy band has been assigned to a charge-transfer (CT) exciton state delocalized over more than one perylene molecule. The solution electronic absorption spectra of many perylene derivatives show well-structured vibronic transitions in the S_1 state. By analogy, for PPEI, the 0–0 transition is located at ~500 nm, and the lower energy peak centered at 550 nm is assigned to a CT state.[43]

The characteristics of the vapor-annealed PPEI thin-film absorption are similar to those observed in related thin films of PTCDA.[43,44] After a short exposure to CH_2Cl_2 vapor the 550 nm peak appears red-shifted by 60 nm and broadened, resulting in the appearance of a peak centered at 610 nm.[26] The peak at 500 nm, assigned to the singlet manifold, remains nearly constant, while the peak at 610 nm increases in amplitude with increased annealing time. In the film studied here there is very little change in the PPEI absorption spectrum upon further annealing (Figure 5a), suggesting that the PPEI crystals formed by the initial annealing of the sample do not transform into a new polymorph or that extended annealing does not alter the electronic absorption in these materials. Vapor annealing of the films beyond 30 min does not result in further significant changes in the spectrum of PPEI. This observation is also supported by the AFM data above. The spectrum of the annealed film is consistent with a crystalline film as previously observed.[9,19,26] The shift of the CT band to lower energy and the subsequent broadening of this peak upon crystallization have
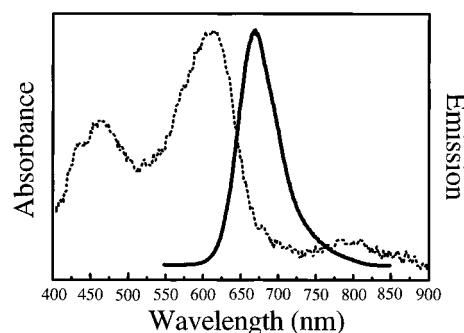
been attributed to extended delocalization of the excited state as the perylene units stack within the crystal.[45,46] Large shifts in energy of the optical absorption bands are evidence of the strong intermolecular interactions that occur in the solid state. The changes observed here in the optical absorption spectrum of PPEI are consistent with previous studies that used changes in absorption spectra as an indicator of crystallinity within vapor-deposited films.[9,19,26]

The absorption spectrum of TiOPc as a function of annealing time in methylene chloride vapor is also shown in Figure 5b. The visible Q-band absorption of phthalocyanines occurs in the 600–750 nm range and arises from the π–π* in-plane polarized charge-transfer transition of the phthalocyanine ring system.[6] This peak is most pronounced in the absorption spectrum of the unannealed films. The peaks at 450 and 610 nm are due to the absorption of PPEI, which is present in the bilayer. The annealed TiOPc films show a broad absorption from 750 to 900 nm with a maximum at 860 nm. The evolution of the optical absorption spectrum of TiOPc upon vapor annealing with CH_2Cl_2 is qualitatively similar to the evolution observed in PPEI films.[26] As with PPEI, the appearance of the low-energy band observed at 860 nm upon vapor annealing has been assigned as a charge-transfer exciton state.[27]

Fluorescence Spectra. Representative fluorescence and absorption spectra for solvent vapor-annealed PPEI are displayed in Figure 6. The fluorescence data presented in this paper involve optical excitation of PPEI at 430 nm. The fluorescence spectra displayed have not been corrected for the detector response. A Stokes shift of nearly 80 nm is observed for the annealed PPEI crystalline materials. The fluorescence line shape is invariant with excitation wavelength between 400 and 600 nm. Excitation into either the S_1 (~500 nm) or CT state (~600 nm) results in the same fluorescence response. This result suggests that the S_1 and CT state are in thermal equilibrium and that emission results from the lower energy CT state after relaxation of the S_1 manifold.[43] The low-energy tail of the observed fluorescence (>750 nm) has been attributed to self-trapped excitons that result from the strong exciton–phonon coupling found in perylene crystals.[43,44] However, it is likely that there is a distribution of energy levels, or defect sites, even in the best organic crystals. As a result, an exciton will lose energy with time as it migrates through the crystal, falling into ever deeper traps and shifting its emission to the red. For this reason, high-energy excitons will have a very short "diffusion length" and will lose energy before they diffuse to any significant extent. This effect has been seen for the polycrystalline PPEI films studied by Gregg et al.[13]

Absorption of light by the PPEI layer produces singlet CT excitons by a radiationless decay mechanism from the S_1 state. In the absence of a TiOPc layer, the PPEI layer is highly

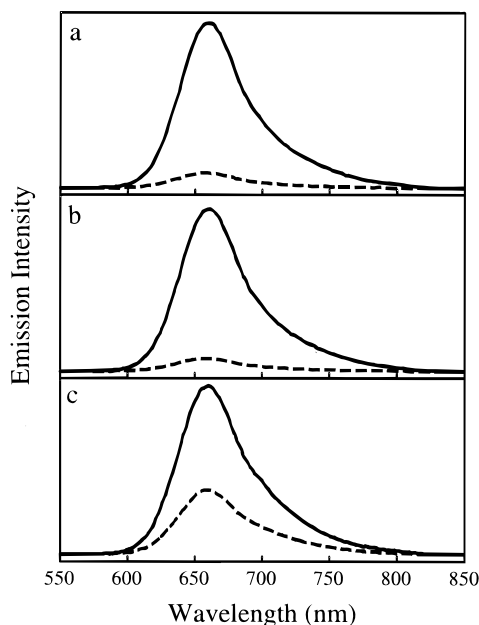**4522** *J. Phys. Chem. B, Vol. 102, No. 23, 1998*

Conboy et al.

Figure 7. Steady-state fluorescence emission spectra of PPEI and TiOPc/PPEI bilayers as a function of postdeposition solvent vapor annealing time. Corresponding topographical images are shown in Figure 2. The top curve in each plot is the emission spectra of the PPEI-only film (solid line), with the emission spectra of the TiOPc/PPEI bilayer represented by the lower curve (long dash). (a) Emission spectra prior to bilayer solvent annealing, (b) after 30 min, and (c) after an additional 120 min.

fluorescent. The total fluorescence intensity increases slightly upon exposure of the PPEI films to methylene chloride vapor, as compared to the unannealed sample. As the films are further annealed and the crystals grow in size, no additional change in the fluorescence intensity is observed.

The efficiency of charge separation at the PPEI–TiOPc interface can be inferred from the fluorescence data. At the interface, exciton dissociation occurs by injection of an electron into the perylene layer and a hole into TiOPc layer (i.e., electron transfer from TiOPc to PPEI).[10] This electron-transfer process at the PPEI–TiOPc interface is an efficient quenching mechanism for the CT fluorescence of the PPEI layer. The steady-state fluorescence spectra of the PPEI and TiOPc/PPEI thin films as a function of annealing time are displayed in Figure 7 (corresponding topographical images are shown in Figure 2). Comparison of the unannealed TiOPc/PPEI interface and the annealed TiOPc/PPEI interface shows that after prolonged solvent annealing the fluorescence quenching decreases. The highest degree of quenching is found for the unannealed film at 92%, determined by integrating the total emission spectra. The quenching efficiency drops to 67% for the fully annealed samples. The fully annealed TiOPc/PPEI film shown in Figure 3, where isolated nanocrystallites of TiOPc are sparsely located at the step edges of the PPEI crystals, also shows ∼65% quenching. Previous NSOM investigations performed on the upside-down film (PPEI/TiOPc displayed in Figure 4) similarly show ∼60% fluorescence quenching.[14]

Fluorescence Lifetime Measurements. Table 1 shows the fluorescence lifetimes and fraction of fluorescence quenched from lifetime and steady-state measurements for the bilayer films shown in Figures 2–4. For the thin films shown in Figure 2, moderate annealing times produce very little change in both observed emission decay rates and overall emission intensities. In fact, time-resolved and steady-state emission intensities remain almost unchanged during the first 30 min of bilayer

TABLE 1: Bilayer TiOPc/PPEI Films: Fluorescence Lifetimes, Fraction Fluorescence Quenched from Time Resolved, and Steady-State Measurement

bilayer annealing time	τ_{avg} (ps)[a]	$(1 - \tau/\tau_0)$[b]	$(1 - q/q_0)$[c]
0 min/Figure 2b	60 ± 9	0.83 ± 0.10	0.91 ± 0.05
30 min/Figure 2d	60 ± 9	0.82 ± 0.10	0.92 ± 0.05
120 min/Figure 2f	115 ± 16	0.65 ± 0.12	0.62 ± 0.05
120 min/Figure 3	~130	~0.65	~0.65
(PPEI/TiOPc)/Figure 4[d]		~0.40	~0.60

[a] Emission decays were fit to a three-exponential, convolved with our instrument response function. Spatial resolution of the lifetime measurement is approximately 4 μm² and in all cases represents a contribution from several PPEI crystals. [b] τ_0 is simply τ_{avg} for PPEI crystals in the absence of TiOPc and corresponds to regions of the sample displayed in the left-hand column of the topographical images in Figure 2. [c] Integrated emission intensities were collected with an illuminated area of approximately 5000 μm² in the sample regions displayed in Figure 2. q_0 represents the integrated emission intensity observed for PPEI crystals in the absence of TiOPc. [d] From NSOM measurements in ref 10.
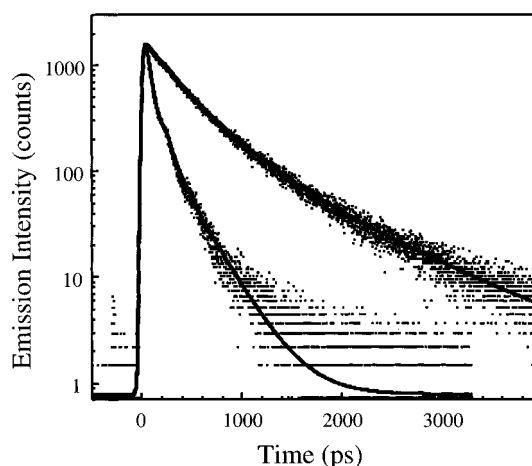

Figure 8. Representative emission decay curves for PPEI and TiOPc/PPEI thin films. The solid lines through the data represent a convolution of the instrument response function with an exponential decay of the form $I = A_1 \exp[t/\tau_1] + A_2 \exp[t/\tau_2] + A_3 \exp[t/\tau_3]$.

annealing. This is while dramatic changes are occurring in the morphology of the bilayer assembly. As seen in the AFM image (Figure 2d), after 30 min of solvent vapor annealing the bilayer surface is covered with numerous small crystallites obscuring the underlying PPEI crystals. After extended annealing (Figure 2f), the fraction of fluorescence quenched is substantially reduced. Bilayer TiOPc/PPEI films displaying isolated crystallites of TiOPc at the edges of PPEI (Figure 3) show similar degrees of quenching compared to the films in Figure 2f.

Representative emission decays for PPEI and a TiOPc/PPEI bilayer are presented in Figure 8. The solid lines in Figure 8 represent a convolution of the instrument response function (50 ps fwhm) with an exponential decay of the form $I = A_1 \exp$-$[t/\tau_1] + A_2 \exp[t/\tau_2] + A_3 \exp[t/\tau_3]$. The average fluorescence lifetime on glass is $\tau_{avg} = 350$ ps compared to $\tau_{avg} = 60$ ps with a slightly annealed TiOPc overlayer. This decrease in PPEI emission lifetime reflects an 82% change in the fluorescence decay observed for PPEI in contact with TiOPc versus a PPEI-only film. Near-field scanning optical microscopy measurements further corroborate that quenching of PPEI fluorescence occurs as a result of contact with TiOPc (see below and elsewhere[14]).

Comparison of the time-resolved and steady-state emission data indicates that some fluorescence quenching occurs faster than our instrument response (<50 ps). This unresolved fast
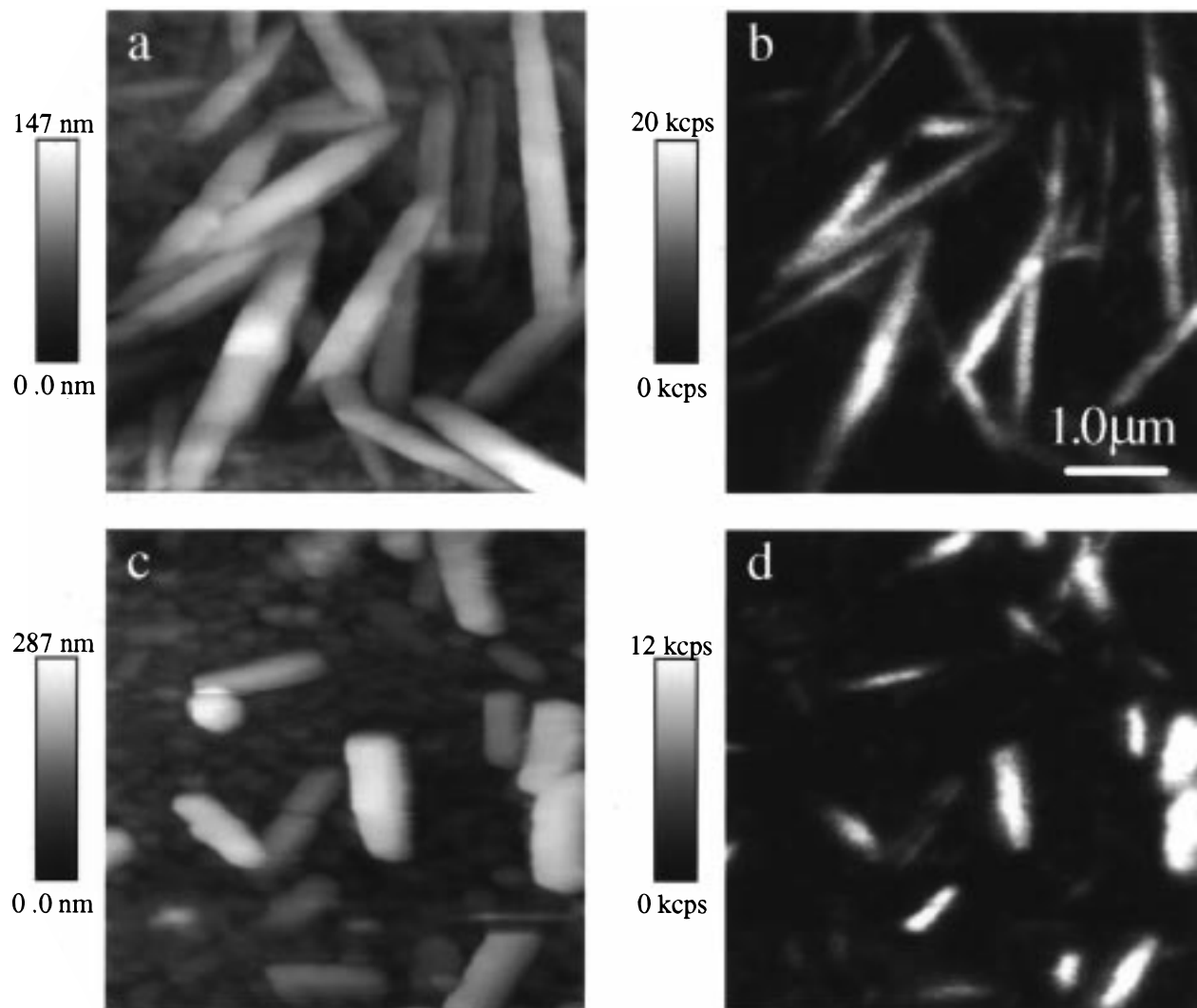
Molecular Semiconductor Films

J. Phys. Chem. B, Vol. 102, No. 23, 1998 **4523**

Figure 9. Shear-force topographical images and NSOM fluorescence images of a TiOPc/PPEI bilayer assembly after extended solvent vapor annealing (analogous to the sample described in Figure 2e,f). Comparison of the PPEI-only region of the sample (a) and (b), with the TiOPc/PPEI bilayer region (c) and (d) confirms that the large crystallites observed are PPEI, not TiOPc.

component of the emission decay could be the result of excitons in the crystal that are quenched at the interface in <30 ps. Excitons created near the interface for which the transit time to the interface would be extremely short and/or extremely fast exciton migration rates toward the interface would result in an unresolvable component of the emission decay that would not be well represented in our fit to the data.

Emission decays were obtained over a broad spectral region (>575 nm). This procedure was used since the nature of the CT state undergoing charge separation and subsequent quenching of the emissive state at the TiOPc interface is at present unclear. Studies of the analogous PTCDA system suggest that several CT states in the crystal may be responsible for the observed fluorescence.[43,44] In addition, the possibility of self-trapped states within the crystal may also be contributing to the observed transients. To our knowledge, no study has been conducted to determine the number of states or which of these states are responsible for charge separation at the interface. Hence, in this study, the complete emission band was collected in an attempt to minimize bias for one state or another. It is also possible that by measuring the transients using the total emission band we have inadvertently biased the lifetime data by inclusion of emissive states that are not quenched by TiOPc. Specifically, self-trapped excitons or low-energy defect sites may not allow for exciton migration to the interface where quenching

by TiOPc can occur. To investigate this proposal, emission transients were obtained for the low-energy region of the emission (>750 nm) and revealed the same quantitative decrease in PPEI emission lifetimes summarized in Table 1. If a significant fraction of the observed emission did originate from self-trapped excitons or low-energy defect sites, the emission lifetimes obtained on the low-energy side of the emission band would not be affected by the changes in morphology of the TiOPc at the interface. The changes in the morphology at the interface are responsible for the changes in the observed lifetimes.

NSOM Experiments. NSOM is effective in determining local molecular structure, orientation, and concentrations in PPEI−TiOPc bilayer films.[14] Figure 9a−d shows the NSOM shear-force topographical images and corresponding NSOM fluorescence images for a single layer of PPEI and the TiOPc/PPEI bilayer (same sample as Figure 2e,f). The near-field fluorescence images of Figure 9 were obtained with circularly polarized 420 nm excitation in order to ensure near equal excitation of the anisotropically absorbing PPEI crystals in a particular image area. All emission at wavelengths greater than 550 nm was collected and imaged onto the detector. In our experiment the TiOPc is nonemissive. The regions of high emission intensity correspond to the large crystalline structures in both parts b and d of Figure 9. This observation confirms

that these larger crystallites are indeed PPEI and not TiOPc. The smaller nanocrystalline regions of Figure 9c are predominately composed of nanocrystalline TiOPc and to a lesser extent nanocrystalline PPEI, since some emission is observed in these regions as seen in Figure 9d.

The fluorescence intensity along the larger PPEI crystals grown in the presence of a TiOPc overlayer (Figure 9d) appears uniform in comparison to the fluorescence intensity variations seen along crystals of PPEI grown on a TiOPc underlayer (fluorescence image shown elsewhere[14]). In the previous study, polarized transmission and fluorescence NSOM showed that the variations in fluorescence intensity were due to local differences in the concentration of PPEI along the crystals. In effect, as PPEI crystals grow on a crystalline TiOPc surface, the lower faces of the PPEI crystals conform to the small nanocrystals of TiOPc. High-resolution AFM images of PPEI/TiOPc bilayer systems are shown in Figure 4. Contrastingly, the uniform fluorescence intensity seen for the PPEI crystals in the annealed TiOPc/PPEI bilayer (Figure 9d) indicates that these crystals reside on the glass and do not have nanocrystals of TiOPc beneath them. TiOPc surrounds the PPEI crystal and likely forms a contact similar to that seen in Figure 3.

Interfacial Charge-Transfer Fluorescence Quenching. The process of solvent annealing alters the morphology of the PPEI and TiOPc layers and the interfacial contact. However, even though this process may result in reduced contact between layers, moderate solvent annealing is known to improve photovoltaic device performance.[13,15,25,26] This has been attributed to increased exciton diffusion lengths, charge carrier mobilities, charge separation efficiencies, and alterations of the optical/electronic band structures. In nearly amorphous bilayer films (both PPEI and TiOPc layers), small crystalline domains and large numbers of domain boundaries present barriers to exciton and charge migration. The boundaries potentially can function as low-energy trap sites and recombination centers that limit exciton and charge migration distances. However, very effective contact is achieved in thin amorphous bilayer systems. As amorphous films are annealed the contact between the layers is reduced, and the charge-transfer quenching efficiency decreases.

Efficient fluorescence quenching observed in TiOPc/PPEI bilayer films (Figure 2b,d) is attributed to effective contact between the layers and results from nearly uniform coverage of the TiOPc on the crystalline PPEI. Exciton migration is expected to be very efficient in crystalline PPEI films.[13] Moreover, exciton migration has been shown to be 3-dimensional in nature in PPEI crystals.[14] Consequently, excitons created anywhere in single PPEI crystals can migrate effectively to the interface and be quenched by electron transfer from TiOPc. This is reflected in the 92% loss in fluorescence intensity observed in these films. Amorphous TiOPc/PPEI (Figure 2b) and the slightly annealed TiOPc/PPEI (Figure 2d) show comparable fluorescence quenching. Uniform nanocrystalline regions of TiOPc are observed on the upper surface of the PPEI crystals shown in Figure 2d. TiOPc crystals in this case, however, must be closely spaced such that there is not a significant amount of energy wasting as excitons migrate to the nanocrystalline contact points. The crystalline nature of both layers is not only beneficial for exciton migration, but likely gives rise to increased charge carrier mobility in both layers, resulting in more effective charge separation (i.e., generation of free charge carriers). Thus, crystalline morphology in both layers is expected to result in improved photovoltaic response in a working device.

Extended solvent vapor annealing leads to reduced interfacial contact between the TiOPc and PPEI layers as shown in the high-resolution topographical images (Figures 2f, 3, and 4). These images nicely display how Ostwald ripening can create void spaces in the contact between layers. The observed fluorescence quenching efficiency is ~65% for all three of these bilayers. Excitons created in the crystalline PPEI layer must migrate to the widely separated contact points to undergo charge transfer. The reduced fluorescence quenching, manifested as greater total emission intensities and longer lifetimes, is therefore a result of energy wasting as excitons migrate to the dispersed interfacial contact points.

Although the bilayer in Figure 2f displays a different polymorph of PPEI than is present in any of the other films, the observed fluorescence quenching mechanism is likely similar to the other films, namely, charge transfer at TiOPc contact points. This is substantiated by the observation of comparable fluorescence quenching efficiencies in all three bilayer films and similarly well-spaced localized TiOPc contact points as observed in the NSOM and AFM data. These observations suggest that the change in the morphology of PPEI may play a lesser role in the exciton-quenching dynamics than the quality of the interface between PPEI and the emission quencher TiOPc.

Conclusions

High-resolution atomic force microscopy (AFM) has been used in conjunction with NSOM and conventional fluorescence and absorption spectroscopy to determine the effect of solvent vapor annealing on the nanoscopic structure and charge-transfer efficiency of PPEI–TiOPc bilayer films. AFM data reveal that solvent vapor annealing leads to the evolution of crystals from the initially amorphous vacuum-deposited films. The relatively uniform size distribution of crystals has been interpreted as an Ostwald ripening process of the films upon exposure to methylene chloride vapor. In the presence of a TiOPc overlayer, for very thin bilayer assemblies, solvent vapor annealing produces a previously unobserved polymorphic form of PPEI. The more common needlelike crystals of PPEI are formed (i) in the absence of TiOPc, (ii) when preannealed TiOPc is the sublayer, or (iii) when thicker preannealed PPEI films are used as the sublayer. Unannealed films and slightly annealed films of TiOPc on crystalline PPEI were shown to effectively quench PPEI fluorescence by >90%. Efficient fluorescence quenching was attributed to effective contact between the layers and nearly uniform coverage of the TiOPc on the crystalline PPEI. Extended annealing was shown to extensively restructure the layers and reduce the interfacial contact between the TiOPc and PPEI. AFM and NSOM measurements clearly show the existence of localized, widely dispersed TiOPc contact points in highly annealed TiOPc/PPEI (two different polymorphs) and PPEI/TiOPc bilayers. Each of these bilayers showed decreased fluorescence quenching efficiencies. The inefficient quenching was attributed to energy wasting as excitons in the PPEI crystals migrate to the separated TiOPc charge-transfer quenching points. Furthermore, crystalline/crystalline TiOPc/PPEI bilayers were obtained which displayed >90% fluorescence quenching. The crystalline nature of both layers not only is beneficial in promoting long-range exciton migration but also is expected to give rise to increased charge carrier mobility in both layers and more effective generation of free charge carriers. Such crystalline/crystalline interfaces are implicated as important targets for device applications.

Molecular Semiconductor Films

J. Phys. Chem. B, Vol. 102, No. 23, 1998 **4525**

References and Notes

(1) Tang, C. W.; Van Slyke, S. A. *Appl. Phys. Lett.* **1987**, *51*, 913.

(2) Tang, C. W.; Van Slyke, S. A.; Chen, C. H. *J. Appl. Phys.* **1989**, *65*, 3615.

(3) Reinecker, P.; Haken, H.; Wolf, H. C. E. *Organic Molecular Aggregates*; Springer-Verlag: Berlin, 1983.

(4) Simon, J.; Andre, J. J. *Molecular Semiconductors*; Springer-Verlag: Berlin, 1985.

(5) Loutfy, R. O.; Sharp, J. U.; Hsiao, C. K.; Ho, R. *J. Appl. Phys.* **1981**, *52*, 5218.

(6) Law, K.-Y. *Chem. Rev.* **1993**, *93*, 449.

(7) Wohrle, D.; Meissner, D. *Adv. Mater.* **1991**, *3*, 129.

(8) Danziger, J.; Dodelet, J.-P.; Lee, P.; Nebesny, K. W.; Armstrong, N. R. *Chem. Mater.* **1991**, *3*, 821.

(9) Debe, M. K.; Kam, K. K.; Liu, J. C.; Poirier, R. J. *J. Vac. Sci. Technol. A* **1988**, *6*, 1907.

(10) Popovic, Z. D.; Hor, A.-M.; Loutfy, R. O. *Chem. Phys.* **1988**, *127*, 451.

(11) Umeda, M.; Yokoyama, M. *J. Appl. Phys.* **1997**, *81*, 6179.

(12) Umeda, M.; Shimada, T.; Aruga, T.; Niimi, T.; Sasaki, M. *J. Phys. Chem.* **1993**, *97*, 8531.

(13) Gregg, B. A.; Sprague, J.; Peterson, M. W. *J. Phys. Chem. B* **1997**, *101*, 5362.

(14) Adams, D. M.; Kerimo, J.; Olson, E. J. C.; Zaban, A.; Gregg, B. A.; Barbara, P. F. *J. Am. Chem. Soc.* **1997**, *119*, 10608.

(15) Gregg, B. A. *Appl. Phys. Lett.* **1995**, *67*, 1271.

(16) Gregg, B. A.; Fox, M. A.; Bard, A. J. *J. Phys. Chem.* **1990**, *94*, 1586.

(17) Gregg, B. A.; Kim, Y. I. *J. Phys. Chem.* **1994**, *98*, 2412.

(18) Geacintov, N.; Pope, M.; Kallman, H. *J. Chem. Phys.* **1966**, *45*, 2639.

(19) Tamizhmani, G.; Dodelet, J. P.; Cote, R.; Gravel, D. *Chem. Mater.* **1991**, *3*, 1046.

(20) Borsenberger, P. M.; Weiss, D. S. *Organic Photoreceptors for Imaging Systems*; Marcel Dekker: New York, 1993.

(21) Gastonguay, L. G.; Veilleux, G.; Cote, R.; Saint-Jacques, R. G.; Dodelet, J. P. *J. Electrochem. Soc.* **1992**, *139*, 337.

(22) Borsenberger, P. M.; Regan, M. T.; Staudenmayer, W. J. Multi-Active Photoconductive insulating elements and method for their manufacture US Patent Number 4,618,560, 1986.

(23) Hor, A.-M.; Loutfy, R. O. *Thin Solid Films* **1983**, *106*, 291.

(24) Loutfy, R. O.; Hor, A.-M.; Kazmaier, P.; Tam, M. *J. Imaging Sci.* **1989**, *33*, 151.

(25) Tsuzuki, T.; Kuwabara, Y.; Noma, N.; Shirota, Y. *Jpn. J. Appl. Phys.* **1996**, *35*, L447.

(26) Gregg, B. A. *J. Phys. Chem.* **1996**, *100*, 852.

(27) Saito, T.; Sisk, W.; Kobayashi, T.; Suzuki, S.; Iwayanagi, T. *J. Phys. Chem.* **1993**, *97*, 8026.

(28) Klofta, T. J.; Rieke, P. C.; Linkous, C. A.; Buttner, W. J.; Nanthakumar, A.; Mewborn, T. D.; Armstrong, N. R. *J. Electrochem. Soc.* **1985**, *132*, 2134.

(29) Vanden Bout, D. A.; Kerimo, J.; Higgins, D. A.; Barbara, P. F. *Acc. Chem. Res.* **1997**, *30*, 204.

(30) Higgins, D. A.; Kerimo, J.; Vanden Bout, D. A.; Barbara, P. F. *J. Am. Chem. Soc.* **1996**, *118*, 4049.

(31) Higgins, D. A.; Vanden Bout, D. A.; Kerimo, J.; Barbara, P. F. *J. Phys. Chem.* **1996**, *100*, 13794.

(32) Higgins, D. A.; Barbara, P. F. *J. Phys. Chem.* **1995**, *99*, 3.

(33) Pohl, D. W.; Denk, W.; Lanz, M. *Appl. Phys. Lett.* **1984**, *44*, 651.

(34) Betzig, E.; Trautman, J. K.; Harris, T. D.; Weiner, J. S.; Kostelak, R. L. *Science* **1991**, *251*, 1468.

(35) Honigmann, B.; Horn, D. *SCI Monogr.* **1973**, *38*, 283.

(36) Zhuang, P.; Cheng, P.; Zhao, Y. *Huagong Xuebao* **1986**, 445.

(37) Hanitzsch, E.; Kahlweit, M. *Z. Phys. Chem.* **1968**, *57* (3−6), 145.

(38) Boistelle, R.; Astier, J. P. *J. Cryst. Growth* **1988**, *90*, 14.

(39) Dunning, W. J. *Sci. Monogr.* **1973**, *38*, 3.

(40) Ostwald, W. *Z. Phys. Chem.* **1900**, *34*, 295.

(41) van Zeggeren, F.; Benson, G. C. *Can. J. Chem.* **1957**, *35*, 1150.

(42) Dundon, M. L. *J. Am. Chem. Soc.* **1923**, *45*, 2658.

(43) Bulovic, V.; Burrows, P. E.; Forrest, S. R.; Cronin, J. A.; Thompson, M. E. *Chem. Phys.* **1996**, *210*, 1.

(44) Bulovic, V.; Forrest, S. R. *Chem. Phys.* **1996**, *210*, 13.

(45) Klebe, G.; Graser, F.; Hadicke, E.; Berndt, J. *Acta Crystallogr.* **1989**, *B45*, 69.

(46) Kazmaier, P. M.; Hoffman, R. *J. Am. Chem. Soc.* **1994**, *116*, 9684.